Table 2 Primers for amplification and sequencing of exon-1's in *UGT1A8, 1A7, 1A3,* and 5′-flanking region of *1A9*

	Direction	*Gene*	*Primer name*	*Sequences*
1st amplification	Forward	*1A8*	UGT1A8ZF	5′-GTGGCTGGTACTCATTTTTCC-3′
	Reverse		UGT1A8ZR	5′-CTTCCAAACCCAACATCTCTAA-3′
	Forward	*1A9-7*	UGT1A9-7ZF	5′-TCTTGATTGTCCTCCATTGAGT-3′
	Reverse		UGT1A9-7ZR	5′-ACCAAGCAACCATACTCATAGG-3′
2nd amplification	Forward	*1A8*	UGT1A8-1stF	5′-AGAATGTGGAAGTAGAGCGG-3′
	Reverse		UGT1A8-1stR	5′-TTAGCAAAAAAGGAAAGTTCAA-3′
	Forward	*1A9* 5′-Flank	UGT1A9pro-248F1st	5′-TTGAGACAGAGTCGTGCTGTT-3′
	Reverse		UGT1A9pro-608R1st	5′-GCAAAGCCACAGGTCAGC-3′
	Forward	*1A7*	UGT1A71stF	5′-AAATGAATGAATAAGTACACGCC-3′
	Reverse		UGT1A71stR	5′-GGAAGTTTCATTTCTTACTGTGG-3′
	Forward	*1A3*	UGT1A3-1stF	5′-GTGAGCACAGGGTCAGACGTGT-3′
	Reverse		UGT1A3-1stR	5′-TTACAAACATTCGTGTCTACTT-3′
Sequencing	Forward	*1A8* Exon1	UGT1A8Ex1Fseq1	5′-TATGACAGGATAAATACACGCC-3′
	Forward	*1A8* Exon1	UGT1A8Ex1Fseq3	5′-ACTCAACCTCATACACTCTGGAG-3′
	Forward	*1A8* Exon1	UGT1A8Ex1Fseq2	5′-TGCTCCTCTTTCCTATGTCC-3′
	Reverse	*1A8* Exon1	UGT1A8Ex1Rseq1	5′-AACTTCGTACTTGTGCTTTCCA-3′
	Reverse	*1A8* Exon1	UGT1A8Ex1Rseq2	5′-ACTGGCAAAATAAATGTTCCTC-3′
	Reverse	*1A8* Exon1	UGT1A8Ex1Rseq3	5′-GCAACAAATGAAAATGTCAAATC-3′
	Forward	*1A9* 5′-Flank	UGT1A9pro-275Fseq	5′-GCTCTCGCAAGGATTGGG-3′
	Reverse	*1A9* 5′-Flank	UGT1A9pro-275Rseq	5′-CTTATGGTCTTTGCCTTGGG-3′
	Forward	*1A7* Exon1	UGT1A7F3-2	5′-TTTGAGGGCAGGTTCTATCTG-3′
	Reverse	*1A7* Exon1	UT1A71R3	5′-CAAAAACCATGAACTCCCGG-3′
	Forward	*1A7* Exon1	UT1A71F4	5′-TGGCAACTGGGAAGATCAC-3′
	Reverse	*1A7* Exon1	UT1A71R4	5′-GGACATAGGAAAGAGGAGCAG-3′
	Forward	*1A7* Exon1	UT1A71F5	5′-CTCCCTCCCCTCTGTGGTC-3′
	Reverse	*1A7* Exon1	UT1A71R5	5′-GCACTGGCTTTCCCTGATGAC-3′
	Forward	*1A7* Exon1	UGT1A7F6-2	5′-GAGGAACATTTATTTTGCCC-3′
	Reverse	*1A7* Exon1	UT1A71R6	5′-TACATATCAACAAGAGCTGC-3′
	Forward	*1A3* Exon1	UGT1A3seqF1	5′-GTGTTTTTCAAGATAGTC-3′
	Reverse	*1A3* Exon1	UGT1A3seqR1	5′-GCACATGGCGATCAAATTC-3′
	Forward	*1A3* Exon1	UGT1A3seqF2	5′-AGGCAGTGGTCCTCACCCCAGA-3′
	Reverse	*1A3* Exon1	UGT1A3seqR2	5′-AAGCATGGCAAATGTAGGACAGG-3′
	Forward	*1A3* Exon1	UGT1A3seqF3	5′-CCCTTCCTCCTATATTCCTAGA-3′
	Reverse	*1A3* Exon1	UGT1A3-1stR	5′-TTACAAACATTCGTGTCTACTT-3′

sequences). The PCR primers for the 2nd amplification of *1A10* and *1A9* were described previously.[37,38] Exon 1 in *1A3* and the promoter region of *1A9* were first directly amplified from genomic DNA (100 ng) using Ex-Taq as in the 2nd round of PCR described below. The second round of PCR consisted of one cycle at 94°C for 5 min, followed by 30 cycles of 94°C for 30 s, 55°C for 1 min, and 72°C for 2 min, and then a final extension for 7 min at 72°C. These PCR products were then treated with a PCR Product Pre-Sequencing Kit (USB Co., Cleveland, OH, USA) and directly sequenced on both strands using an ABI BigDye Terminator Cycle Sequencing Kit (Applied Biosystems, Foster City, CA, USA) and the primers listed in Table 2 (see 'Sequencing'). The excess dye was removed by a DyeEx96 kit (Qiagen, Hilden, Germany), and the eluates were analyzed on an ABI Prism 3700 DNA Analyzer (Applied Biosystems). All the SNPs were confirmed by repeating the PCR on genomic DNA and sequencing the newly generated PCR products.

Genotyping (pyrosequencing)

Genotyping was performed by pyrosequencing, except for *UGT1A4* 31C>T (R11W), 127delA (43fsX22: frameshift from codon 43 resulting in the termination at the 22nd codon, codon 65), 142T>G (L48V), 175delG (59fsX6), 271C>T (R91C), 325A>G (R109G), and IVS+1G>T, and *1A9* −126_−118 T9>T10 or T11, which were genotyped by direct sequencing because these polymorphisms were not clearly determined by pyrosequencing. Fragments were directly amplified from genomic DNA (10–15 ng) by Ex-Taq (1 U) with amplification primer pairs (either primer was biotinylated) (Table 3). The PCR conditions consisted of 1 cycle at 94°C for 5 min, followed by 50 cycles of 94°C for 30 s, 55°C for 30 s (except for *UGT1A* 1598A>C (H533P), in which annealing was carried out at 58°C for 45 s), and 72°C for 30 s. Primers for *1A1* −3279T>G, −40_−39 insTA, 211G>A (G71R), 247T>C (F83L), 686C>A (P229Q), and 1456T>G (Y486D) in common exon 5 were described

Table 3 Primers in pyrosequencing

	Gene	*Detected variation*	*Amino-acid change*	*Primer name*	*Direction*	*Length*	*Sequences*
Amplification	*UGT1A8*	518C>G	A173G	UGT1A8PyroF	Forward	387 bp	5′-bTACGAAGTTTGTTTTCTCTATTTCT-3′
				UGT1A8PyroR2b[a]	Reverse		5′-CTATTTCTAGGGCATTTTTGG-3′
	UGT1A10	4G>A, 177G>A, 200A>G	A2T, M59I, E67G	UGT1A10Pyro1F2-2	Forward	378 bp	5′-GGTCAGGTTTTGTGCCTGTAC-3′
				UGT1A10Pyro1R2b[a]	Reverse		5′-bATTGAGCATGGGCGAAAA-3′
	UGT1A10	605C>T	T202I	UGT1A10Pyro2F	Forward	123 bp	5′-CTTTCCTATGTCCCCAATGA-3′
				UGT1A10Pyro2Rb[a]	Reverse		5′-bGGCATTTCTAAAAAGATACTGG-3′
	UGT1A9	422C>G, 726T>G, 766G>A	S141C, Y242X, D256N	UGT1A9PyroF	Forward	589 bp	5′-TATTAATGGGTTCATACAATGACA-3′
				UGT1A9PyroRb[a]	Reverse		5′-bTTTTTTAATTTCCAAAGGTGAAG-3′
	UGT1A7	387T>G, 391C>A, 392G>A, 622T>C	N129K, R131K, W208R	UGT1A7PyroF	Forward	364 bp	5′-TATTAACAAGTTCATCCAATGGTA-3′
				UGT1A7PyroRb[a]	Reverse		5′-bTCTAAGACATTTTTGAAAAAATAGG-3′
	UGT1A6	19T>G, 269G>A, 308C>A	S7A, R90H, S103X	UGT1A6-1pyroF2	Forward	354 bp	5′-TTTAACTCTTTCCAGGATGGC-3′
				UGT1A6-1pyroR1b[a]	Reverse		5′-bCTGTACTCTGTCTGAGGAGCAGT-3′
	UGT1A6	541A>G, 552A>C	T181A, R184S	UGT1A6-2pyroF1b[a]	Forward	180 bp	5′-bACCATCTGTGTACCTCTTCAGG-3′
				UGT1A6-2pyroR1	Reverse		5′-AGACAATAAAATAGATAGGGCTCC-3′
	UGT1A3	17A>G, 31T>C	Q6R, W11R	UGT1A3pyroF1	Forward	379 bp	5′-CACTCTGTCTTCCAATTACACGT-3′
				UGT1A3pyroR3b[a]	Reverse		5′-bTCCACGAAATGGCATAGGT-3′
	UGT1A3	133C>T, 140T>C	R45W, V47A	UGT1A3pyroF1b[a]	Forward	379 bp	5′-bCACTCTGTCTTCCAATTACACGT-3′
				UGT1A3pyroR3	Reverse		5′-TCCACGAAATGGCATAGGT-3′
	UGT1A	1091C>T[b]	P364L[b]	UT1AP364L-F	Forward	226 bp	5′-TGAAACTCAGAGATGTAACTGCTG-3′
				UT1AP364L-Rb[a]	Reverse		5′-bCAGAAGTCATTTCCAGAACATTC-3′
	UGT1A	1598A>C[b]	H533P[b]	exon5-F	Forward	242 bp	5′-TGGGTGGAGTTTGTGATGA-3′
				bExon5R-H533P[a]	Reverse		5′-bCCTTATTTCCCACCCACTT-3′
	UGT1A 3′-UTR[c]	1813C>T[b], 1941C>G[b], 2042C>G[b]	*1B*[d]	UGT1AEx5-1BPyroFb[a]	Forward	332 bp	5′-bATTTGAATATGTATCGTGCCC-3′
				UGT1AEx5-1BPyroR	Reverse		5′-CATTCATTCATTTCACCTACACT-3′
Pyrosequencing	*UGT1A8*	518C>G	A173G	UGT1A8c518gPF			5′-CGCCAGGGGAATAG-3′
	UGT1A10	4G>A	A2T	UGT1A10g4aPF			5′-GGCTGCAGTTCTCTCA-3′
	UGT1A10	177G>A	M59I	UGT1A10g177aPF			5′-GCATGAGGTGGTTGTAG-3′
	UGT1A10	200A>G	E67G	UGT1A10a200gPF			5′-TGAGTTGGCAACTGG-3′
	UGT1A10	605C>T	T202I	UGT1A10c605tPF			5′-GGTTCTCAGATGCCATG-3′
	UGT1A9	422C>G	S141C	UGT1A9c422gPF			5′-AGAATACTTAAAGGAGAGT-3′
	UGT1A9	726T>G	Y242X	UGT1A9t726gPF			5′-AAACACCTGTTACGGAG-3′
	UGT1A9	766G>A	D256N	UGT1A9g766aPF			5′-GGTTGTTGCGAACG-3′
	UGT1A7	387T>G, 391C>A, 392G>A	N129K, R131K	UGT1A7387-392PF			5′-ATTGCAGGAGTTTGTTTA-3′
	UGT1A7	622T>C	W208R	UGT1A7c622tPF			5′-TTCAAGGAGAGAGTA-3′
	UGT1A6	19T>G	S7A	UGT1A6-1t19gPseq-F			5′-CCTGCCTCCTTCGC-3′
	UGT1A6	269G>A	R90H	UGT1A6-1g269aPseq-F			5′-AAGAAGAGCTGAAGAACC-3′
	UGT1A6	308C>A	S103X	UGT1A6-1c308aPseq-F			5′-AACAATCACTTTGCTGAG-3′
	UGT1A6	541A>G, 552A>C	T181A, R184S	UGT1A6-2a552cPseq-R			5′-GGACACAGGGTCTGG-3′
	UGT1A3	17A>G, 31T>C	Q6R, W11R	UGT1A3a17g-seqF			5′-TGGCCACAGGACTC-3′
	UGT1A3	133C>T, 140T>C	R45W, V47A	UGT1A3t140cPseq-R			5′-ATGGAGCTCCCGCAA-3′
	UGT1A	1091C>T[b]	P364L[b]	UGT1A1P364LPseqF			5′-TTTGCATCTCAGGTCAC-3′
	UGT1A	1598A>C[b]	H533P[b]	Exon5-1598F-Page			5′-CACAAATCCAAGACCC-3′
	UGT1A 3′-UTR[c]	1813C>T[b]	*1B*[d]	UGT1AEx5c1813tPseqR			5′-TCCTGATCAAAGACACC-3′
	UGT1A 3′-UTR[c]	1941C>G[b]	*1B*[d]	UGT1AEx5c1941gPseqR			5′-CAGTAGGGGCAGC-3′
	UGT1A 3′-UTR[c]	2042C>G[b]	*1B*[d]	UGT1AEx5c2042gPseqR			5′-TGGCACCTATGAAGCA-3′

[a]b: biotinylated.
[b]The positions of nucleotide and protein were numbered as those of *UGT1A1*.
[c]UTR: untranslated region.
[d]1813C>T, 1941C>G, and 2042C>G found in the 3′-UTR were named haplotype *1B*.[19]

previously.[39] Biotinylated single-stranded DNA fragments were generated as described previously.[39] Briefly, PCR products were mixed with streptavidin beads for 10 min. The beads were transferred to a MultiScreen-HV Plate (Millipore Corporation, Billerica, MA, USA), and the buffer was removed by vacuum. DNA attached to the beads was denatured, washed twice, and then suspended in 20 mM Tris-acetate containing 2 mM Mg-acetate (pH 7.6). After transferring to a 96-well PSQ plate (Pyrosequencing AB, Uppsala, Sweden), 10 pmol of the sequencing primer (PAGE-purified grade) (Table 3) for SNP analysis was added to the single-stranded fragments. The mixture was incubated at 95°C for 2 min, and then cooled to room temperature for annealing. An automated pyrosequencing instrument, the PSQ™96MA (Pyrosequencing AB), and the PSQ 96 SNP reagent kit (Pyrosequencing AB) were used to perform the genotyping. To validate the typing methods, the results for 48 samples were confirmed to be identical to those obtained by direct sequencing (data not shown).

LD and haplotype analysis

Hardy–Weinberg equilibrium analysis and LD analysis were performed using SNPAlyze software (version 3.2). (Dynacom Co. Ltd., Yokohama, Japan), and pairwise two-dimensional maps between SNPs were obtained for the $|D'|$, χ^2, and r^2 values. Some of the haplotypes were unambiguously determined from the subjects with homozygous SNPs at all sites or a heterozygous SNP at only one site. Separately, the diplotype configurations (combination of haplotypes) were inferred by an expectation-maximization-based program, LDSUPPORT, which determines the posterior probability distribution of the diplotype configuration for each subject based on the estimated haplotype frequencies.[40]

The diplotype configurations of the subjects were inferred with probability (certainty) values over 0.96 for 184, 191, and 188 out of 196 subjects in the *UGT1A8-1A10* block (*Block 8/10*), the *1A9-1A7-1A6* block (*Block 9/6*), and the *1A3-1A1* block (*Block 3/1*), respectively. The *Block 4* (*1A4*) haplotypes were described previously.[21] Note that the predictability for the extremely rare haplotypes inferred from only one subject is known to be low in some cases. Haplotype analysis was also performed among the representative SNPs in *Block 9/6*, *Block 4*, and *Block 3/1* by LDSUPPORT software.

Abbreviations

LD	*linkage disequilibrium*
PCR	*polymerase chain reaction*
SN-38	*7-ethyl-10-hydroxycamptothecin*
SNP	*single nucleotide polymorphism*
UGT	*UDP-glucuronosyltransferase*
UTR	*untranslated region*

Acknowledgments

This study was supported in part by the Program for Promotion of Fundamental Studies in Health Sciences and by the Health and Labour Sciences Research Grants from Ministry of Health, Labour and Welfare, and the grant from the Japan Health Sciences Foundation. We thank Ms Chie Sudo for her secretarial assistance.

DUALITY OF INTEREST

None declared.

References

1 Radominska-Pandya A, Czernik PJ, Little JM. Structural and functional studies of UDP-glucuronosyltransferases. *Drug Metab Rev* 1999; **31**: 817–899.
2 Tukey RH, Strassburg CP. Genetic multiplicity of the human UDP-glucuronosyltransferases and regulation in the gastrointestinal tract. *Mol Pharmacol* 2001; **59**: 405–414.
3 Gong QH, Cho JW, Huang T, Potter C, Gholami N, Basu NK *et al.* Thirteen UDPglucuronosyltransferase genes are encoded at the human UGT1 gene complex locus. *Pharmacogenetics* 2001; **11**: 357–368.
4 Metz RP, Ritter JK. Transcriptional activation of the UDP-glucuronosyltransferase 1A7 gene in rat liver by aryl hydrocarbon receptor ligands and oltipraz. *J Biol Chem* 1998; **273**: 5607–5614.
5 Guillemette C. Pharmacogenomics of human UDP-glucuronosyltransferase enzymes. *Pharmacogenomics J* 2003; **3**: 136–158.
6 Guillemette C, Ritter JK, Auyeung DJ, Kessler FK, Housman DE. Structural heterogeneity at the UDP-glucuronosyltransferase 1 locus: functional consequences of three novel missense mutations in the human UGT1A7 gene. *Pharmacogenetics* 2000; **10**: 629–644.
7 Gagne JF, Montminy V, Belanger P, Journault K, Gaucher G, Guillemette C. Common human UGT1A polymorphisms and the altered metabolism of irinotecan active metabolite 7-ethyl-10-hydroxycamptothecin (SN-38). *Mol Pharmacol* 2002; **62**: 608–617.
8 Huang YH, Galijatovic A, Nguyen N, Geske D, Beaton D, Green J *et al.* Identification and functional characterization of UDP-glucuronosyltransferases UGT1A8*1, UGT1A8*2 and UGT1A8*3. *Pharmacogenetics* 2002; **12**: 287–297.
9 Elahi A, Bendaly J, Zheng Z, Muscat JE, Richie Jr JP, Schantz SP *et al.* Detection of UGT1A10 polymorphisms and their association with orolaryngeal carcinoma risk. *Cancer* 2003; **98**: 872–880.
10 Jinno H, Saeki M, Saito Y, Tanaka-Kagawa T, Hanioka N, Sai K *et al.* Functional characterization of human UDP-glucuronosyltransferase 1A9 variant, D256N, found in Japanese cancer patients. *J Pharmacol Exp Ther* 2003; **306**: 688–693.
11 Jinno H, Saeki M, Tanaka-Kagawa T, Hanioka N, Saito Y, Ozawa S *et al.* Functional characterization of wild-type and variant (T202I and M59I) human UDP-glucuronosyltransferase 1A10. *Drug Metab Dispos* 2003; **31**: 528–532.
12 Villeneuve L, Girard H, Fortier LC, Gagne JF, Guillemette C. Novel functional polymorphisms in the UGT1A7 and UGT1A9 glucuronidating enzymes in Caucasian and African-American subjects and their impact on the metabolism of 7-ethyl-10-hydroxycamptothecin and flavopiridol anticancer drugs. *J Pharmacol Exp Ther* 2003; **307**: 117–128.
13 Ehmer U, Vogel A, Schutte JK, Krone B, Manns MP, Strassburg CP. Variation of hepatic glucuronidation: novel functional polymorphisms of the UDP-glucuronosyltransferase UGT1A4. *Hepatology* 2004; **39**: 970–977.
14 Nagar S, Zalatoris JJ, Blanchard RL. Human UGT1A6 pharmacogenetics: identification of a novel SNP, characterization of allele frequencies and functional analysis of recombinant allozymes in human liver tissue and in cultured cells. *Pharmacogenetics* 2004; **14**: 487–499.
15 Jinno H, Tanaka-Kagawa T, Hanioka N, Saeki M, Ishida S, Nishimura T *et al.* Glucuronidation of 7-ethyl-10-hydroxycamptothecin (SN-38), an active metabolite of irinotecan (CPT-11), by human UGT1A1 variants, G71R, P229Q, and Y486D. *Drug Metab Dispos* 2003; **31**: 108–113.
16 Judson R, Stephens JC, Windemuth A. The predictive power of haplotypes in clinical response. *Pharmacogenomics* 2000; **1**: 15–26.
17 Kohle C, Mohrle B, Munzel PA, Schwab M, Wernet D, Badary OA *et al.* Frequent co-occurrence of the TATA box mutation associated with Gilbert's syndrome (UGT1A1*28) with other polymorphisms of the

UDP-glucuronosyltransferase-1 locus (UGT1A6*2 and UGT1A7*3) in Caucasians and Egyptians. *Biochem Pharmacol* 2003; **65**: 1521–1527.
18 Carlini LE, Meropol NJ, Bever J, Andria ML, Hill T, Gold P *et al.* UGT1A7 and UGT1A9 polymorphisms predict response and toxicity in colorectal cancer patients treated with capecitabine/irinotecan. *Clin Cancer Res* 2005; **11**: 1226–1236.
19 Sai K, Saeki M, Saito Y, Ozawa S, Katori N, Jinno H *et al.* UGT1A1 Haplotypes associated with reduced glucuronidation and increased serum bilirubin in irinotecan-administered Japanese cancer patients. *Clin Pharmacol Ther* 2004; **75**: 501–515.
20 Saeki M, Saito Y, Jinno H, Sai K, Kaniwa N, Ozawa S *et al.* Genetic polymorphisms of *UGT1A6* in a Japanese population. *Drug Metab Pharmacokinet* 2005; **20**: 85–90.
21 Saeki M, Saito Y, Jinno H, Sai K, Hachisuka A, Kaniwa N *et al.* Genetic variations and haplotypes of *UGT1A4* in a Japanese population. *Drug Metab Pharmacokinet* 2005; **20**: 144–151.
22 Iwai M, Maruo Y, Ito M, Yamamoto K, Sato H, Takeuchi Y. Six novel UDP-glucuronosyltransferase (UGT1A3) polymorphisms with varying activity. *J Hum Genet* 2004; **49**: 123–128.
23 Kozak M. Recognition of AUG and alternative initiator codons is augmented by G in position +4 but is not generally affected by the nucleotides in positions +5 and +6. *EMBO J* 1997; **16**: 2482–2492.
24 Yamanaka H, Nakajima M, Katoh M, Hara Y, Tachibana O, Yamashita J *et al.* A novel polymorphism in the promoter region of human UGT1A9 gene (UGT1A9*22) and its effects on the transcriptional activity. *Pharmacogenetics* 2004; **14**: 329–332.
25 Lankisch TO, Vogel A, Eilermann S, Fiebeler A, Krone B, Barut A *et al.* Identification and characterization of a functional TATA box polymorphism of the UDP glucuronosyltransferase 1A7 gene. *Mol Pharmacol* 2005; **67**: 1732–1739.
26 Ando M, Ando Y, Sekido Y, Ando M, Shimokata K, Hasegawa Y. Genetic polymorphisms of the UDP-glucuronosyltransferase 1A7 gene and irinotecan toxicity in Japanese cancer patients. *Jpn J Cancer Res* 2002; **93**: 591–597.
27 Huang MJ, Yang SS, Lin MS, Huang CS. Polymorphisms of uridine-diphosphoglucuronosyltransferase 1A7 gene in Taiwan Chinese. *World J Gastroenterol* 2005; **11**: 797–802.
28 Innocenti F, Liu W, Chen P, Desai AA, Das S, Ratain MJ. Haplotypes of variants in the UDP-glucuronosyltransferase1A9 and 1A1 genes. *Pharmacogenet Genomics* 2005; **15**: 295–301.
29 Ciotti M, Basu N, Brangi M, Owens IS. Glucuronidation of 7-ethyl-10-hydroxycamptothecin (SN-38) by the human UDP-glucuronosyltransferases encoded at the UGT1 locus. *Biochem Biophys Res Commun* 1999; **260**: 199–202.
30 Lepine J, Bernard O, Plante M, Tetu B, Pelletier G, Labrie F *et al.* Specificity and regioselectivity of the conjugation of estradiol, estrone, and their catecholestrogen and methoxyestrogen metabolites by human uridine diphospho-glucuronosyltransferases expressed in endometrium. *J Clin Endocrinol Metab* 2004; **89**: 5222–5232.
31 Basu NK, Kubota S, Meselhy MR, Ciotti M, Chowdhury B, Hartori M *et al.* Gastrointestinally distributed UDP-glucuronosyltransferase 1A10, which metabolizes estrogens and nonsteroidal anti-inflammatory drugs, depends upon phosphorylation. *J Biol Chem* 2004; **279**: 28320–28329.
32 Turgeon D, Chouinard S, Belanger P, Picard S, Labbe JF, Borgeat P *et al.* Glucuronidation of arachidonic and linoleic acid metabolites by human UDP-glucuronosyltransferases. *J Lipid Res* 2003; **44**: 1182–1191.
33 Little JM, Kurkela M, Sonka J, Jantti S, Ketola R, Bratton S *et al.* Glucuronidation of oxidized fatty acids and prostaglandins B1 and E2 by human hepatic and recombinant UDP-glucuronosyltransferases. *J Lipid Res* 2004; **45**: 1694–1703.
34 Beutler E, Gelbart T, Demina A. Racial variability in the UDP-glucuronosyltransferase 1 (UGT1A1) promoter: a balanced polymorphism for regulation of bilirubin metabolism? *Proc Natl Acad Sci USA* 1998; **95**: 8170–8174.
35 Sugatani J, Yamakawa K, Yoshinari K, Machida T, Takagi H, Mori M *et al.* Identification of a defect in the UGT1A1 gene promoter and its association with hyperbilirubinemia. *Biochem Biophys Res Commun* 2002; **292**: 492–497.
36 Oguri T, Takahashi T, Miyazaki M, Isobe T, Kohno N, Mackenzie PI *et al.* UGT1A10 is responsible for SN-38 glucuronidation and its expression in human lung cancers. *Anticancer Res* 2004; **24**: 2893–2896.
37 Saeki M, Ozawa S, Saito Y, Jinno H, Hamaguchi T, Nokihara H *et al.* Three novel single nucleotide polymorphisms in UGT1A10. *Drug Metab Pharmacokinet* 2002; **17**: 488–490.
38 Saeki M, Saito Y, Jinno H, Sai K, Komamura K, Ueno K *et al.* Three novel single nucleotide polymorphisms in UGT1A9. *Drug Metab Pharmacokinet* 2003; **18**: 146–149.
39 Saeki M, Saito Y, Jinno H, Tohkin M, Kurose K, Kaniwa N *et al.* Comprehensive UGT1A1 genotyping in a Japanese population by pyrosequencing. *Clin Chem* 2003; **49**: 1182–1185.
40 Kitamura Y, Moriguchi M, Kaneko H, Morisaki H, Morisaki T, Toyama K *et al.* Determination of probability distribution of diplotype configuration (diplotype distribution) for each subject from genotypic data using the EM algorithm. *Ann Hum Genet* 2002; **66**: 183–193.

The FASEB Journal express article 10.1096/fj.05-4034fje. Published online December 22, 2005.

Dimerization and the signal transduction pathway of a small in-frame deletion in the epidermal growth factor receptor

Kazuko Sakai,*,§ Tokuzo Arao,* Tatsu Shimoyama,* Kimiko Murofushi,§ Masaru Sekijima,‖ Naoko Kaji,‖ Tomohide Tamura,† Nagahiro Saijo,† and Kazuto Nishio*,‡

*Shien-Lab, Medical Oncology, and †National Cancer Center Hospital and ‡Pharmacology Division, National Cancer Center Research Institute, Tsukiji 5-1-1, Chuo-ku, Tokyo, Japan; and §Department of Biology, Faculty of Science, Ochanomizu University, Tokyo, Japan; and ‖Mitsubishi Chemical Safety Institute, Ibaraki, Japan

Corresponding author: Kazuto Nishio, Shien-Lab, Medical Oncology, National Cancer Center Hospital, Tsukiji 5-1-1, Chuo-ku, Tokyo 104-0045, Japan. E-mail: knishio@gan2.res.ncc.go.jp

ABSTRACT

A short, in-frame deletional mutant (E746-A750del) is one of the major mutant forms of epidermal growth factor receptor (EGFR) and has been reported to be a determinant of response to EGFR tyrosine kinase inhibitors such as gefitinib and erlotinib. However, the biological and pharmacological functions of mutational EGFR remain unclear. To clarify these biological functions of deletional EGFR, we examined the cellular response to EGF ligand stimulation. Dimerization and phosphorylation of EGFR were observed without any ligand stimulation in the 293(D) cells transfected with deletional EGFR as compared with those transfected with wild-type EGFR (293(W) cells). When the 293(D) cells were exposed to gefitinib, an immunoblotting analysis revealed remarkable inhibition of AKT phosphorylation but not phospho-p44/42 MAPK. To examine the cellular response in a lung cancer cell line intrinsically expressing deletional EGFR, phospho-EGFR, and downstream reactions were monitored under EGF stimulation with a beads-based mulitiplex assay. EGFR and its downstream proteins were constitutively phosphorylated in the PC-9 cells without any ligand stimulation as compared with A549 lung cancer cells expressing wild-type EGFR. In conclusion, deletional EGFR is constitutively active and phosphorylates p44/42 MAPK and AKT in the cells, although the fact that the EGFR phosphorylation in the PC-9 cells is still modulated by EGF stimulation cannot be ignored. Gefitinib-inhibited phospho-AKT predominantly in deletional EGFR expressing cells.

Key words: mutation • gefitinib • tyrosine kinase

Epidermal growth factor receptor (EGFR) belongs to the ErbB family (1) and contains an extracellular ligand-binding domain, a transmembrane domain, and a tyrosine kinase domain. Wild-type EGFR is unphosphorylated and exists as a monomer in the unstimulated conditions. Binding of ligands such as EGF and TGF-α leads to the dimerization of EGFR, phosphorylation of tyrosine residues (2), and stimulation of the phosphorylation pathway downstream. This signaling pathway is considered to be closely related to cellular growth, differentiation, and the development of malignant phenotypes of cancer cells (1, 2). Increased

expression of EGFR and gene amplification of EGFR are often observed in several types of tumors such as lung and breast cancers.

Recently, many small anticancer molecules have been developed that target EGFR. Gefitinib (Iressa) is an orally available EGFR tyrosine kinase inhibitor. Previous clinical studies have demonstrated that EGFR expression levels in tumors did not correlate with the clinical response to gefitinib (3). On the other hand, EGFR mutation in adenocarcinoma of the lung was reported to be a determinant of sensitivity for EGFR tyrosine kinase inhibitors such as gefitinib and erlotinib (4, 5). To date, over 30 types of EGFR mutation have been reported in lung cancer. The in-frame, 15 base deletional mutation (delE746-A750 type deletion) is one of the most common of these EGFR mutations. We previously demonstrated that overexpression of deletional EGFR increased the cellular sensitivity to tyrosine kinase inhibitors targeting EGFR in human HEK293 cells in vitro (6). However, it remains unclear how deletional EGFR alters dimerization and the downstream signaling pathways from these heterodimers. Recently, Tracy et al. demonstrated that another major mutant EGFR (L858R) altered signal transduction downstream (7). In addition, it has been suggested that the L858R mutation is a hyper-response to ligand stimulation (7). We hypothesized that the deletional EGFR is constitutively active. The aim of this study was to clarify the downstream of the signaling and its function of the deletional EGFR.

Technically, a beads-based multiplex assay (Bio-Plex phosphoprotein assay) (8) allowed us to analyze numbers of phosphoproteins simultaneously after ligand stimulation.

MATERIALS AND METHODS

Reagents

Gefitinib (Iressa, ZD1839) was provided by AstraZeneca (Cheshire, UK).

Cell culture

The human embryonic kidney HEK293 cell line and human nonsmall-cell lung cancer (NSCLC) cell line A549 and cervix epitheloid cancer cell line HeLa were obtained from the American Type Culture Collection (Manassas, VA) and were cultured in RPMI 1640 medium supplemented with 10% FBS. The human NSCLC cell line PC-9 was established at the Tokyo Medical University (9, 10), and was maintained in RPMI 1640 medium (Sigma, St. Louis, MO) supplemented with 10% heat-inactivated fetal bovine serum (FBS; Life Technologies, Rockville, MD).

Plasmid construction and transfection

The construction of the mock expression plasmid vector (empty vector) and of the wild-type of EGFR and the 15-bp deletional EGFR (delE746-A750 type deletion) vectors that posses the same deletion site observed in PC-9 cells has been described in another paper in detail (6, 11, 12). The plasmids were transfected into the HEK293 cells, and the transfectants were selected by Zeosin (Sigma). The stable transfectants (pooled cultures) of the empty vector, wild type of EGFR, and its deletion mutant were designated as 293(M), 293(W), and 293 (D) cells, respectively.

Reverse-transcription PCR

Five micrograms of total RNA from each cultured cell line was converted to cDNA with a GeneAmp RNA-PCR kit (Applied Biosystems, Foster City, CA). The primers used for the PCR were EGFR (forward), 5′-AAGTTAAAATTCCCGTCGCTATCA-3′ and (reverse) 5′-GAGCCAATATTGTCTTTGTGTTCC-3′. PCR amplification consisted of 28 cycles (95°C for 45 s, 57.5°C for 30 s, and 72°C for 45 s) followed by incubation at 72°C for 7 min. The RT-PCR products were analyzed with a 2100 Bioanalyzer and DNA 500 kit (Agilent Technologies, Waldbronn, Germany).

Chemical cross-linking

After treatment with or without EGF (Sigma), monolayer cells were washed twice with ice-cold phosphate buffered saline containing 0.33 mM $MgCl_2$ and 0.9 mM $CaCl_2$ (PBS(+)) and chemically cross-linked for 20 min at room temperature with freshly prepared 1.5 mM bis(sulfosuccinimidyl) suberate (BS^3, Pierce, Rockford, IL). To terminate the reaction, a final concentration of 20 mM glycine was added for an additional 5 min. For immunoblot analysis, the cells were washed twice with ice-cold PBS(+) and lysed with M-PER mammalian protein extraction reagent (Pierce). The lysate was centrifuged at 20,000 *g* for 10 min, and the protein concentration of the supernatant was measured with a BCA (bicinchoninic acid) protein assay (Pierce).

Ligand stimulation

After reaching 70–80% confluence, cultured cells were stimulated with EGF, TGF-α, and HB-EGF for 10 min under nonstarved conditions or serum-starved conditions. The cells were washed twice with ice-cold PBS(+), and lysed for immunoblotting.

Drug treatment

After reaching 70–80% confluence, cultured cells, were exposed to various concentrations of gefitinib and stimulated or not stimulated with EGF (100 ng/ml) for 10 min under nonstarved conditions or serum-starved conditions. The cells were washed twice with ice-cold PBS(+) and lysed for immunoblotting.

Immunoblot analysis

Immunoblot analysis was performed as described previously (12). Equivalent amounts of protein were separated by electrophoresis on a SDS-PAGE and transferred to a polyvinylidene difluoride (PVDF) membrane (Millipore, Bedford, MA). The membrane was probed with a mouse monoclonal antibody against EGFR (Transduction Lab, San Diego, CA), a phospho-EGFR antibody (specific for Tyr1068), p44/42 mitogen-activated protein kinase (p44/42 MAPK), phospho-p44/42 MAPK, AKT, phospho-AKT, nuclear factor-κB (NF-κB) inhibitor α (IκB-α), and phospho-IκB-α antibody (Cell Signaling Technology, Beverly, MA) as the first antibody, followed by a horseradish peroxidase-conjugated secondary antibody. The bands were visualized with electrochemiluminescence (ECL, Amersham, Piscataway, NJ), and images of blotted patterns were analyzed with NIH image software (National Institutes of Health, Bethesda, MD).

Phosphoprotein assay

A panel of phosphoproteins was measured in duplicate using a bead-based mulitiplex assay (Bio-Plex phosphoprotein assay, Bio-Rad, Hercules, CA), according to the manufacturer's instructions (8, 13). The EGFR-transfected 293 cells and NSCLC cells cultured in the serum-free medium for 24 h were stimulated by the addition of EGF at a final concentration of 100 ng/ml for the indicated time intervals. After incubation, the cells were rinsed with ice-cold Cell Wash Buffer and collected. The lysate was centrifuged at 1,700 *g* for 20 min. The protein concentration was calculated with a DC (detergent compatible) protein assay (Bio-Rad). The Bio-Plex assay was customized to detect and quantify phosphoproteins of EGFR, p44/42 MAPK, activating transcription factor 2 (ATF-2), c-Jun N-terminal kinase (JNK), p38 mitogen-activated protein kinase (p38 MAPK), IκB-α, and signal transducer and activator of transcription 3 (STAT-3). The prepared first antibody with coupled beads was captured under 96-well plates, and samples (17.5 μg each) were incubated overnight at room temperature. Samples were incubated with biotin-labeled detection antibodies followed by further incubation with the fluorescence-labeled avidin reporter. The level of phosphoproteins bound to the beads was indicated by the intensity of the reporter signal. The signal was measured with Bio-Plex Manager software (Bio-Rad) interfaced with a Bio-Plex Reader (Bio-Rad). In this assay, we used the lysates of untreated HeLa cells as the background control for all phosphoprotein assays provided by the Bio-Plex phosphoprotein assay (14). This experiment was repeated in duplicate.

RESULTS

Dimerization and phosphorylation of wild-type EGFR and deletional EGFR

The EGFR expression level in the 293 cells transfected with the empty vector (293(M)), wild-type EGFR (293(W)), and deletional EGFR (293(D)), in the A549 and PC-9 NSCLC cells, and in the HeLa cervix epitheloid cancer cells were determined by RT-PCR and immunoblot analysis (Fig. 1). The PCR products were separated into wild-type EGFR (upper band) and deletion mutant EGFR (lower band) by the different lengths of the sequences. Overexpression of EGFR was detected in the 293(W) and 293(D) cells. Only a small amount of intrinsically EGFR was detected in 293(M) cells by RT-PCR. We sequenced exon 19 and 20 of EGFR in HEK293 cells, but no mutations were detected (data not shown). A high level of EGFR expression was detected in the PC-9 cells, and a moderate level was detected in the A549 and HeLa cells. The EGFR protein levels closely matched the mRNA expression levels in all cells.

Dimerization of EGFR, the first step in the EGFR signaling pathway, was examined by chemical cross-linking. The 293(M), 293(W), and 293(D) cells were treated with EGF (10 ng/ml) for 10 min under nonstarved conditions (Fig. 2*A*). Cells were incubated with the cross-linking reagent BS^3. Dimerization and phosphorylation of EGFR were determined by immunoblot with anti-EGFR and anti-phospho EGFR antibodies. Dimerization and expression of EGFR were not detected in the 293(M) cells. Dimerized EGFR with a molecular weight of ~400 kDa was detected in the 293(W) cells. Increased phosphorylation and dimerization of the deletional EGFR were detected without EGF stimulation in the 293(D) cells by the chemical cross-linking and immunoblot assay, respectively. When the cells were stimulated with the EGF ligand (10 ng/ml for 10 min), increased phospho-EGFR dimers were observed in the 293(W) cells, whereas no response of EGFR to EGF was observed in the 293(D) cells. We quantified the levels of monomeric and dimerized EGFR in the 293(W) and 293(D) cells densitometrically under nonstarved conditions (Fig. 2*A*, right). In the

293(W) cells, the dimer/monomer ratio was increased ~40% by the addition of EGF. Addition of EGF slightly increased the dimer/monomer ratio (~20%) in the 293(D) cells.

We investigated the dimerization and phosphorylation status of EGFR in the EGFR-transfected cell lines under serum-starved conditions (Fig. 2*B*). The transfected cells were exposed by EGF (10 ng/ml for 10 min) after serum starvation for 24 h. No expression of EGFR dimer or monomer was detected in the 293(M) cells. Addition of EGF resulted in an increase in dimerized and phosphorylated EGFR in the 293(W) cells. Dimerization and phosphorylation of the deletional EGFR were detected in the 293(D) cells in the absence of EGF after serum starvation. Expression of dimerized EGFR in the 293(D) cells was unchanged by EGF stimulation. These findings demonstrated that the deletional mutant EGFR was constitutively dimerized and phosphorylated without any ligand stimulation even under starved conditions and are consistent with the results under nonstarved conditions (Fig. 2*A*). The ratio of dimerized to monomeric EGFR in 293(W) and 293(D) cells was analyzed densitometrically under serum-starved conditions (Fig. 2*B*, right). The dimer/monomer ratio in the 293(W) cells was markedly increased (~3 fold) by addition of EGF. Under unstimulated conditions, the dimer/monomer ratio of the 293(D) cells was higher than that of the 293(W) cells, and the ratio was unchanged by addition of EGF.

These results suggest that the cells expressing the wild-type of EGFR responded to EGF for their dimerization and phosphorylation and that the deletion mutant of EGFR was dimerized and phosphorylated constitutively without any ligand stimulation.

Phosphorylation of EGFR, p44/42 MAPK, and AKT in the EGFR-transfected 293 cells

The p44/42 MAPK and AKT are major downstream targets of EGFR. We examined the phosphorylation status of p44/42 MAPK and AKT with EGF addition in the transfectants. The transfected cells were treated with EGF (10 ng/ml) for 10 min under nonstarved conditions (Fig. 3*A*). The phosphorylation levels of EGFR in the 293(D) cells were higher without any ligand stimulation than that of the 293(W) cells. Phospho-EGFR in the 293(W) cells was increased after EGF stimulation. These findings are consistent with Fig. 2. Even under unstimulated conditions, increased phosphorylation of p44/42 MAPK and AKT was observed in the 293(D) cells. In the 293(W) cells, increased phosphorylation of p44/42 MAPK and AKT was observed with the addition of EGF especially p44/42 MAPK was remarkably phosphorylated. On the other hand, in the 293(D) cells, phosphorylation of p44/42 MAPK and AKT was not increased with the addition of EGF. We quantified the phosphorylation levels of p44/42 MAPK and AKT densitometrically in the transfectants in response to EGF. The addition of EGF increased phosphorylation of p44/42 MAPK in the 293(M) cells (~3.4 fold) and in the 293(W) cells (~2.5 fold) (Fig. 3*B*), suggesting no difference in response in regard to p44/42 MAPK to EGF. Increased phosphorylation of AKT in the 293(M) cells (~2.1 fold) and in the 293(W) cells (~1.3 fold) was observed. By contrast, EGF decreased the phosphorylation of p44/42 MAPK and AKT in the 293(D) cells ~30% and ~20% (Fig. 3*C*). These findings suggest that the p44/42 MAPK and AKT pathways are activated in cells expressing the deletional EGFR without ligand stimulation.

Next, we examined the dose-dependent response of EGFR status in the transfected cells to the other ligands, TGF-α, and HB-EGF, after serum starvation (Fig. 4). The hyperphosphorylated EGFR in the 293(D) cells was unchanged by stimulation with these ligands either. By contrast, a dose-dependent increase in EGFR phosphorylation was observed in the 293(W) cells in response to stimulation by TGF-α and HB-EGF. Both HB-EGF and EGF strongly increased EGFR

phosphorylation in the 293(W) cells compared with TGF-α. We also examined the downstream in response to these ligands. In the 293(W) cells, increased phosphorylation of p44/42 MAPK and AKT was observed in response to addition of the ligands (EGF, TGF-α, and HB-EGF). p44/42 MAPK was markedly phosphorylated by the ligands. In the 293(D) cells, addition of ligands further increased p44/42 MAPK phosphorylation. The AKT phosphorylation in the 293(D) cells was unchanged by stimulation with these ligands. These findings are consistent with the data in Fig. 3*A*, and suggest that the p44/42 MAPK and AKT pathways are both activated in cells constitutively expressing the deletional EGFR.

Effect of gefitinib on phosphorylation of EGFR, p44/42 MAPK, and AKT in the EGFR-transfected 293 cells

Previously, we demonstrated that 293(D) cells were hypersensitive to EGFR-targeted tyrosine kinase inhibitors such as gefitinib and ZD6474, as compared with 293(W) cells (6). To examine the specific action of these tyrosine kinase inhibitors on deletional EGFR signal transduction, we exposed the 293 transfectants to gefitinib, and its cellular response was examined under nonstarved conditions with an immunoblot analysis (Fig. 5*A*). In the 293(W) cells, phosphorylation of p44/42 MAPK was not inhibited by exposure to a low dose of gefitinib (0.01 μM) but phosphorylation of AKT was inhibited by exposure to gefitinib (0.01 μM). In contrast, exposure to gefitinib decreased phospho-EGFR in the 293(D) cells that are hypersensitive to gefitinib. Phosphorylation of AKT was completely inhibited by 0.01 μM gefitinib exposure, while the inhibition of p44/42 MAPK phosphorylation was not remarkable in the 293(D) cells. The effect of 0.01 μM gefitinib on phosphorylated p44/42 MAPK and AKT in the transfectents measured densitometrically. p44/42 MAPK phosphorylation in the 293(M) and 293(W) cells was unaltered by gefitinib exposure for 3 h, but it decreased in the 293(D) cells (~20%) (Fig. 5*B*). Gefitinib increased phosphorylation of AKT ~1.3 fold in the 293(M) cells. Gefitinib inhibited AKT phosphorylation was ~70% in the 293(W) cells, and decreased it ~99% in the 293(D) cells (Fig. 5*C*).

We examined the dose-dependent effect of gefitinib (0.02, 0.2, 2 μM) on EGFR and its downstream signaling in all of the transfectants under serum-starved conditions. Phosphorylation of EGFR was not detected in the 293(W) cells under the 24 h serum-starved conditions, and gefitinib had no effect on it (Fig. 6*A*). Hyperphosphorylation of EGFR was dose dependently inhibited by gefitinib in the 293(D) cells. p44/42 MAPK and AKT were slightly phosphorylated in the 293(W) cells, and their degree of phosphorylation was unaltered by exposure to gefitinib. By contrast, gefitinib dose-dependently decreased phosphorylation of p44/42 MAPK, and AKT in the 293(D) cells. Under EGF stimulation (Fig. 6*B*), gefitinib dose-dependently decreased phosphorylation of EGFR, p44/42 MAPK, and AKT in the 293(W) cells. Phosphorylation of EGFR in the 293(D) cells was completely inhibited by a low concentration of gefitinib (0.02 μM), and phosphorylation of p44/42 MAPK and AKT was dose-dependently inhibited by gefitinib. A low concentration of gefitinib inhibited EGFR phosphorylation and its signal in the 293(D) cells under serum-starved conditions. The phosphorylation of EGFR (and its signal) induced by EGF-addition in the 293(W) cells was inhibited by gefitinib dose dependently.

These data suggest that gefitinib inhibited the AKT signaling pathway more strongly than the p44/42 MAPK signaling pathway in the cells expressing the deletional mutant EGFR.

Response to EGF stimulation in the EGFR-transfected 293 cells

We performed the quantitative phosphoprotein analysis in the 293(W) and 293(D) cells by a beads-based multiplex assay. Downstream from the reaction, we monitored the phosphorylation status of p44/42 MAPK, JNK, and p38 MAPK. We also examined the phosphorylation status of ATF-2 that is located downstream of the MAPK pathway, IκB-α that is a member of the AKT pathway, and STAT-3 that is found downstream of the other signaling pathway. Even under unstimulated conditions, EGFR was hyperphosphorylated in the 293(D) cells but not in the 293(W) cells (Fig. 7*A*). Increased phosphorylation of EGFR was observed in the 293(W) cells (~40 fold), but the phosphorylation of EGFR in the 293(W) cells was much lower than that of the deletional EGFR in the 293(D) cells. IκB-α phosphorylation in the transfected cells was as low as in the HeLa cells, which was used as a negative control (Fig. 7*B*). Under unstimulated conditions, phosphorylation of p44/42 MAPK was greater in the 293(D) cells than in the 293(W) cells (~3 fold) (Fig. 7*C*). A large increase in phosphorylation of p44/42 MAPK in response to the addition of EGF was observed in the 293(W) cells (~15 fold), and a smaller increase was observed in the 293(D) cells (~3.5 fold). These differences in phosphorylated p44/42 MAPK in the 293(W) and 293(D) cells detected in the beads-based multiplex assay are consistent with the result of immunoblotting (Fig. 4). ATF-2 was phosphorylated in the 293(W) cells (~1.5 fold) and 293(D) cells (~1.7 fold) by addition of EGF (Fig. 7*D*). By contrast, the JNK in the 293(W) cells was phosphorylated by addition of EGF (~2 fold), but not phosphorylated in the 293(D) cells (Fig. 7*E*). Phosphorylation of p38 MAPK and STAT-3 was not detected in either type of cell (data not shown). These findings suggest that the p44/42 MAPK and AKT pathways are both phosphorylated without any ligand stimulation in the cells expressing the deletional mutant EGFR.

Response to EGF stimulation in PC-9 cells intrinsically expressing deletional EGFR

The hyperphosphorylation and increased dimerization of deletional EGFR has been demonstrated by ectopic expression of deletional EGFR. To examine whether this phenomenon is also observed in the lung cancer cells intrinsically expressing deletional EGFR, we monitored the phosphorylation of EGFR and its related molecules in the PC-9 cells as compared with the A549 cells. The PC-9 cells and A549 cells express the deletional and wild-type EGFR, respectively. PC-9 cells also express a small amount of wild-type EGFR, and so these cell lines mimic the 293(D) cells. We examined the phosphorylation of EGFR and its downstream signaling molecules in these cells by immunoblotting (Fig. 8*A*). Increased phosphorylation of EGFR was observed in the PC-9 cells even under unstimulated conditions, but not in the A549 cells. The addition of EGF markedly increased the EGFR phosphorylation in the A549 cells compared with the PC-9 cells. Under unstimulated conditions, p44/42 MAPK, and AKT were more phosphorylated in the PC-9 cells than in the A549 cells. Increased phosphorylation of p44/42 MAPK and AKT was observed in the A549 cells after addition of EGF, and p44/42 MAPK was markedly phosphorylated. A small increase in phosphorylation of p44/42 MAPK and AKT was observed in the PC-9 cells in response to the addition of EGF. The increased phosphorylation of IκB-α in the PC-9 cells was observed even under unstimulated conditions. The addition of EGF increased the phosphorylation of IκB-α in the A549 cells but did not alter it in the PC-9 cells. These findings suggest a difference in reactivity to the EGF stimulation between the A549 and PC-9 cells.

Next, examination was performed by a beads-based mulitiplex assay. Increased phosphorylation of EGFR was observed in the PC-9 cells, even under unstimulated conditions, but not in the A549 cells (Fig. 8*B*). These findings are consistent with the results of immunoblotting. EGFR

phosphorylation was markedly increased in the A549 cells (~100-fold), and to a lesser extent increased in the PC-9 cells (~1.4-fold). IκB-α was phosphorylated in the PC-9 cells in the absence of EGF stimulation (Fig. 8*C*), suggesting that the AKT pathway, including IκB-α, was activated in the PC-9 cells expressing deletional EGFR, compared with A549 cells. p44/42 MAPK and ATF-2 were phosphorylated without EGF stimulation in the PC-9 cells compared with the A549 cells (Fig. 8*D* and *E*). A large increase in phosphorylation of p44/42 MAPK and ATF-2 was observed in the A549 cells (~13 fold and ~4.3 fold), and a smaller increase was observed in the PC-9 cells (~3.5-fold and ~1.7-fold). JNK was not phosphorylated in either the A549 or the PC-9 cells. Phosphorylation of JNK in response to EGF stimulation was detected in the A549 cells (~2.6-fold), but not in the PC-9 cells (Fig. 8*F*). No phosphorylation of p38 MAPK and STAT-3 was detected in either cell line (data not shown). These differences in phosphoproteins in the A549 and PC-9 cells are consistent with the results of the beads-based multiplex assay in the EGFR-transfected cells (293(W) and 293(D)) (Fig. 7).

To determine whether there was a significant difference between unstimulated and EGF-stimulated conditions, a statistical analysis was performed using the *t* test. There were significant differences between increased phospho-EGFR, phospho-p44/42 MAPK, phospho-ATF-2, and phospho-JNK ($P>0.01$) in the A549 cells under unstimulated and EGF-stimulated conditions. There were also significant differences in the increased phospho-EGFR, phospho-p44/42 MAPK, phospho-ATF-2, and phospho-IκB-α ($P>0.01$) in the PC-9 cells. The fact that phosphorylation of EGFR, p44/42 MAPK, and ATF-2 in the PC-9 cells is still modulated by EGF stimulation cannot be ignored. This pathway is considered to be preferentially regulated by wild-type EGFR.

DISCUSSION

Previous studies have demonstrated that mutational EGFR is a major factor against determining gefitinib sensitivity. We analyzed the characteristics of deletional EGFR with cells expressing deletional EGFR.

In Fig. 3, phosphorylation of p44/42 MAPK and AKT was increased by EGF in the 293(M) cells, although the EGFR was not overexpressed in these cells. There is a rich cross-talk among the ErbB family that regulates the cellular effects mediated by these receptors. However, ErbB-2 (HER2), ErbB-3 (HER3), and ErbB-4 (HER4) are not expressed, and intrinsic EGFR was weakly expressed in the 293 cells (15). Activation of p44/42 MAPK and AKT in response to EGF might be mediated by the intrinsic EGFR. On the other hand, constitutive activation of EGFR and its downstream pathway is due to the mutant EGFR in the 293(D) cells, suggesting that the mutant EGFR shows a dominant phenotype.

In Fig. 3, p44/42 MAPK and AKT were activated under unstimulated conditions in the 293(D) cells. In these transfectants, EGF did not enhance the phosphorylation of p44/42 MAPK and AKT in contrast to those in the 293(W) cells. The phosphorylation of AKT in these cells seems to be decreased by the addition of EGF (Fig. 3*A*). It can be speculated that EGF negatively regulated the activation of mutant EGFR as a feedback mechanism. It is uncertain whether EGF itself negatively regulates the mutant EGFR. Although the mechanism of this phenomenon remains uncertain, a feedback mechanism might be postulated as a possible explanation. It was reported that leucine-rich repeats and immunoglobulin-like domains 1 (LIRG1) is a negative regulator of EGFR (16) and its transcription was up-regulated by EGF stimulation and caused consequently

degradation of EGFR. Thus the feedback mechanisms, including that mediated by LIRG1, should be clarified in the future study.

The 293(D) cells transfected with deletional EGFR were hypersensitive to the growth-inhibitory effect of EGFR tyrosine kinase inhibitor, including gefitinib (6). AKT phosphorylation was completely suppressed by 0.01 μM gefitinib in the 293(D) cells (Fig. 5). It is suggested that deletional EGFR signaling inclines toward the AKT pathways, and this is correlated with cellular sensitivity to gefitinib. The response to gefitinib in the 293(M) cells cannot be ignored. We speculate that the difference in cell response to gefitinib may be attributable to cell dependency on EGFR in the 293(M), 293(W), and 293(D) cells. Since the 293(W) and 293(D) cells seem to be largely dependent on EGFR, therefore, gefitinib effectively inhibited the AKT phosphorylation in these cells. Cell growth in 293(M) cells, on the other hand, is regulated by other signaling pathways. Then the MAPK and AKT pathways did not respond to gefitinib. In addition, the PC-9 cells intrinsically expressing deletional EGFR were also hypersensitive to gefitinib (11, 17), and the AKT pathway was more sensitively inhibited by gefitinib as compared with p44/42 MAPK pathway (18). These findings are consistent with the evidence seen in the 293(D) cells. The altered downstream pathway in the cells expressing other types of mutant EGFR was previously reported. The L858R and delL747-P753insS were basically unphosphorylated and these mutants were markedly phosphorylated compared with wild-type EGFR by ligand stimulation (4, 5). Activated AKT signaling pathways, but not MAPK pathway was observed in the transfectants of L858R and delL747-P753insS. Taken together, preferential activation of AKT pathway was commonly observed between these EGFR mutant cells. On the other hand, there were some differences between delE746-A750, L858R, and delL747-P753insS; constitutive active in delE746-A750 vs. hyperresponse to ligand stimulation in L858R and delL747-P753insS. These EGFR mutations except for T790M are considered to be "gain of function," although detailed differential function will be clarified in future studies.

We examined the phosphorylation status of EGFR and its downstream events in PC-9 cells intrinsically expressing deletional mutant EGFR in addition to the ectopic expression system. However, the PC-9 cells also express low levels of wild-type of EGFR. It can thus be considered that these cells mimic the 293(D) cells. In the PC-9 cells, IκB-α is activated. IκB-α binds to NF-κB and suppresses this function (19). Kapoor reported that NF-κB activating signal from EGFR is mediated by the PI3-kinase/AKT pathway (20). We used immunoblotting to investigate the phosphorylation of AKT in the PC-9 cells after EGF stimulation. Increased phosphorylation of AKT was induced even under unstimulated conditions and considered that the activation (or phosphorylation) of IκB-α occurred via the AKT pathway machinery. Therefore, the phosphorylation of IκB-α is due to the activation of the AKT pathway in the PC-9 cells.

In the PC-9 cells, increased phosphorylation of p44/42 MAPK and ATF-2 (21, 22) was detected with the addition of EGF. In addition, phosphorylation of IκB-α was also increased by the ligand stimulation in the PC-9 cells, suggesting that this signaling pathway might be mediated by wild-type of EGFR.

We demonstrated that deletional EGFR was hyperphosphorylated and dimerized in a steady state in the 293(D) cells. This mutant is considered to be constitutively active. The activation mutation in EGFR is consistent with that of the c-KIT mutation in GIST that is a target for gleevec (23). The c-KIT mutations in GIST have also been reported as gain-of-function mutations (24). The role of

mutant EGFR and its function in transformation activity and carcinogenesis requires clarification in future studies.

Downstream of the signaling pathway, p44/42 MAPK and AKT pathways are activated in the 293(D) cells, but the AKT pathway was more strongly suppressed by gefitinib. Therefore, the AKT pathway must interact with cellular hypersensitivity to the EGFR targeted tyrosine kinase inhibitor in cells expressing deletional mutant EGFR.

In this study, we focused on the short, in-frame deletional mutant (E746_A750del). Now more than 30 types of mutation have been reported in clinical lung cancer specimens. In the next step, we will examine the biological function of other types of mutants of EGFR differentially, with the aim of selecting clinically meaningful mutations.

ACKNOWLEDGMENTS

This work was supported by funds for the Third Term Comprehensive 10-Year Strategy for Cancer Control and a Grant-in-Aid for Scientific Research from the Ministry of Education, Culture, Sports, Science and Technology of Japan (12217165).

REFERENCES

1. Yarden, Y., and Sliwkowski, M. X. (2001) Untangling the ErbB signalling network. *Nat. Rev. Mol. Cell Biol.* **2**, 127–137

2. Tanner, K. G., and Kyte, J. (1999) Dimerization of the extracellular domain of the receptor for epidermal growth factor containing the membrane-spanning segment in response to treatment with epidermal growth factor. *J. Biol. Chem.* **274,** 35,985–35,990

3. Paez, J. G., Janne, P. A., Lee, J. C., Tracy, S., Greulich, H., Gabriel, S., Herman, P., Kaye, F. J., Lindeman, N., Boggon, T. J., et al. (2004) EGFR mutations in lung cancer: correlation with clinical response to gefitinib therapy. *Science* **304,** 1497–1500

4. Lynch, T. J., Bell, D. W., Sordella, R., Gurubhagavatula, S., Okimoto, R. A., Brannigan, B. W., Harris, P. L., Haserlat, S. M., Supko, J. G., Haluska, F. G., et al. (2004) Activating mutations in the epidermal growth factor receptor underlying responsiveness of non-small-cell lung cancer to gefitinib. *N. Engl. J. Med.* **350,** 2129–2139

5. Sordella, R., Bell, D. W., Haber, D. A., and Settleman, J. (2004) Gefitinib-sensitizing EGFR mutations in lung cancer activate anti-apoptotic pathways. *Science* **305,** 1163–1167

6. Arao, T., Fukumoto, H., Takeda, M., Tamura, T., Saijo, N., and Nishio, K. (2004) Small in-frame deletion in the epidermal growth factor receptor as a target for ZD6474. *Cancer Res.* **64,** 9101–9104

7. Tracy, S., Mukohara, T., Hansen, M., Meyerson, M., Johnson, B. E., and Janne, P. A. (2004) Gefitinib induces apoptosis in the EGFRL858R non-small-cell lung cancer cell line H3255. *Cancer Res.* **64,** 7241–7244

8. Chang, L., and Karin, M. (2001) Mammalian MAP kinase signalling cascades. *Nature* **410,** 37–40

9. Kawamura-Akiyama, Y., Kusaba, H., Kanzawa, F., Tamura, T., Saijo, N., and Nishio, K. (2002) Non-cross resistance of ZD0473 in acquired cisplatin-resistant lung cancer cell lines. *Lung Cancer* **38,** 43–50

10. Nishio, K., Arioka, H., Ishida, T., Fukumoto, H., Kurokawa, H., Sata, M., Ohata, M., and Saijo, N. (1995) Enhanced interaction between tubulin and microtubule-associated protein 2 via inhibition of MAP kinase and CDC2 kinase by paclitaxel. *Int. J. Cancer* **63,** 688–693

11. Koizumi, F., Shimoyama, T., Saijo, N., and Nishio, K. Establishment of a human non-small cell lung cancer cell line resistant to gefitinib. *Int. J. Cancer* **116,** 36–44

12. Koizumi, F., Kanzawa, F., Ueda, Y., Koh, Y., Tsukiyama, S., Taguchi, F., Tamura, T., Saijo, N., and Nishio, K. (2004) Synergistic interaction between the EGFR tyrosine kinase inhibitor gefitinib ("Iressa") and the DNA topoisomerase I inhibitor CPT-11 (irinotecan) in human colorectal cancer cells. *Int. J. Cancer* **108,** 464–472

13. Fulton, R. J., McDade, R. L., Smith, P. L., Kienker, L. J., and Kettman, J. R., Jr. (1997) Advanced multiplexed analysis with the FlowMetrix system. *Clin. Chem.* **43,** 1749–1756

14. Gingrich, J. C., Davis, D. R., and Nguyen, Q. (2000) Multiplex detection and quantitation of proteins on western blots using fluorescent probes. *Biotechniques* **29,** 636–642

15. Chan, S. D., Antoniucci, D. M., Fok, K. S., Alajoki, M. L., Harkins, R. N., Thompson, S. A., and Wada, H. G. (1995) Heregulin activation of extracellular acidification in mammary carcinoma cells is associated with expression of HER2 and HER3. *J. Biol. Chem.* **270,** 22,608–22,613

16. Gur, G., Rubin, C., Katz, M., Amit, I., Citri, A., Nilsson, J., Amariglio, N., Henriksson, R., Rechavi, G., Hedman, H., et al. (2004) LRIG1 restricts growth factor signaling by enhancing receptor ubiquitylation and degradation. *EMBO J.* **23,** 3270–3281

17. Naruse, I., Fukumoto, H., Saijo, N., and Nishio, K. (2002) Enhanced anti-tumor effect of trastuzumab in combination with cisplatin. *Jpn. J. Cancer Res.* **93,** 574–581

18. Ono, M., Hirata, A., Kometani, T., Miyagawa, M., Ueda, S., Kinoshita, H., Fujii, T., and Kuwano, M. (2004) Sensitivity to gefitinib (Iressa, ZD1839) in non-small cell lung cancer cell lines correlates with dependence on the epidermal growth factor (EGF) receptor/extracellular signal-regulated kinase 1/2 and EGF receptor/AKT pathway for proliferation. *Mol. Cancer Ther.* **3,** 465–472

19. Baeuerle, P. A., and Baltimore, D. (1988) I kappa B: a specific inhibitor of the NF-kappa B transcription factor. *Science* **242,** 540–546

20. Kapoor, G. S., Zhan, Y., Johnson, G. R., and O'Rourke, D. M. (2004) Distinct domains in the SHP-2 phosphatase differentially regulate epidermal growth factor receptor/NF-kappaB activation through Gab1 in glioblastoma cells. *Mol. Cell. Biol.* **24,** 823–836

21. Gupta, S., Campbell, D., Derijard, B., and Davis, R. J. (1995) Transcription factor ATF2 regulation by the JNK signal transduction pathway. *Science* **267,** 389–393

22. Morton, S., Davis, R. J., and Cohen, P. (2004) Signaling pathways involved in multisite phosphorylation of the transcription factor ATF-2. *FEBS Lett.* **572,** 177–183

23. Hirota, S., Isozaki, K., Moriyama, Y., Hashimoto, K., Nishida, T., Ishiguro, S., Kawano, K., Hanada, M., Kurata, A., Takeda, M., et al. (1998) Gain-of-function mutations of c-kit in human gastrointestinal stromal tumors. *Science* **279,** 577–580

24. Tarn, C., Merkel, E., Canutescu, A. A., Shen, W., Skorobogatko, Y., Heslin, M. J., Eisenberg, B., Birbe, R., Patchefsky, A., Dunbrack, R., et al. (2005) Analysis of KIT mutations in sporadic and familial gastrointestinal stromal tumors: therapeutic implications through protein modeling. *Clin. Cancer Res.* **11,** 3668–3677

Received April 23, 2005; accepted October 25, 2005

Fig. 1

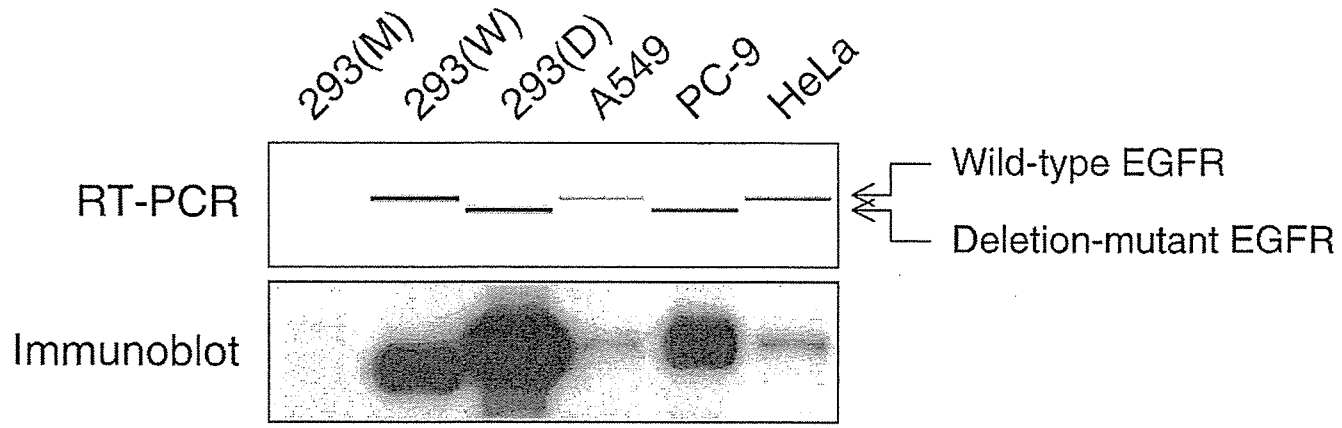

Figure 1. Expression status of epidermal growth factor receptor (EGFR) The EGFR expression level was determined by RT-PCR and immunoblot analysis. The RT-PCR products were analyzed with a 2100 Bioanalyzer. The level of EGFR protein expression was measured by immunoblot with anti-EGFR.

Fig. 2

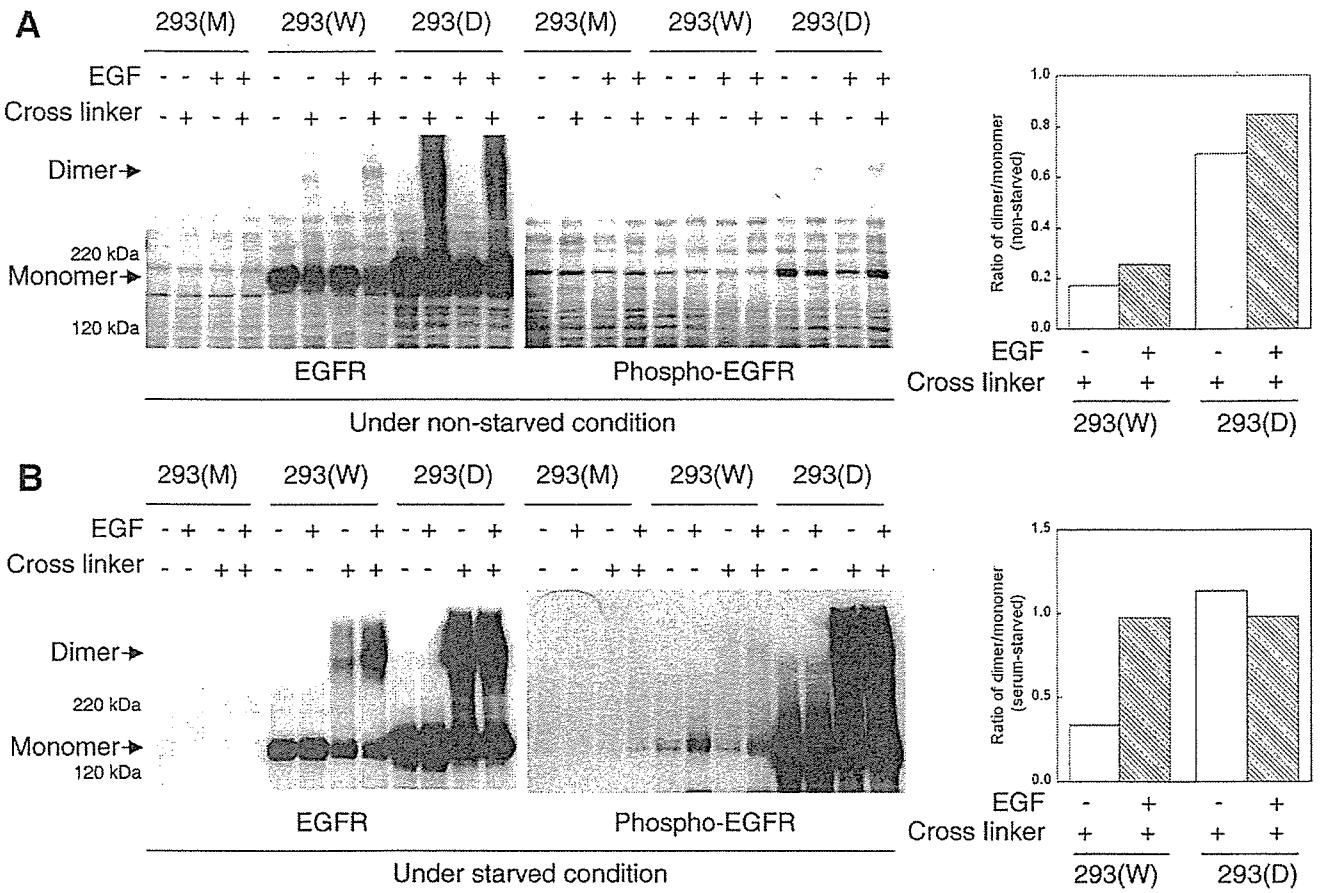

Figure 2. Dimerization and phosphorylation of wild-type EGFR and deletional EGFR. *A*) The transfected cells were treated with or without epidermal growth factor (EGF) (10 ng/ml) for 10 min under nonstarved conditions. After two washes with ice-cold PBS(+), monolayer cells were incubated with the chemical cross-linking reagent BS^3 in PBS(+) as described in the Materials and Methods. Equivalent amounts of protein were separated by 2–15% gradient SDS-PAGE and subjected to immunoblot analysis to detect EGFR and phospho-EGFR. The ratio of dimerized to monomeric EGFR is shown in the ***right panel. B***) The transfected cells were exposed or unexposed to EGF (10 ng/ml) for 10 min after serum starvation. Chemical cross-linking and immunoblotting were performed as described above. The ratio of dimerized to monomeric EGFR is shown in the ***right panel.***

Fig. 3

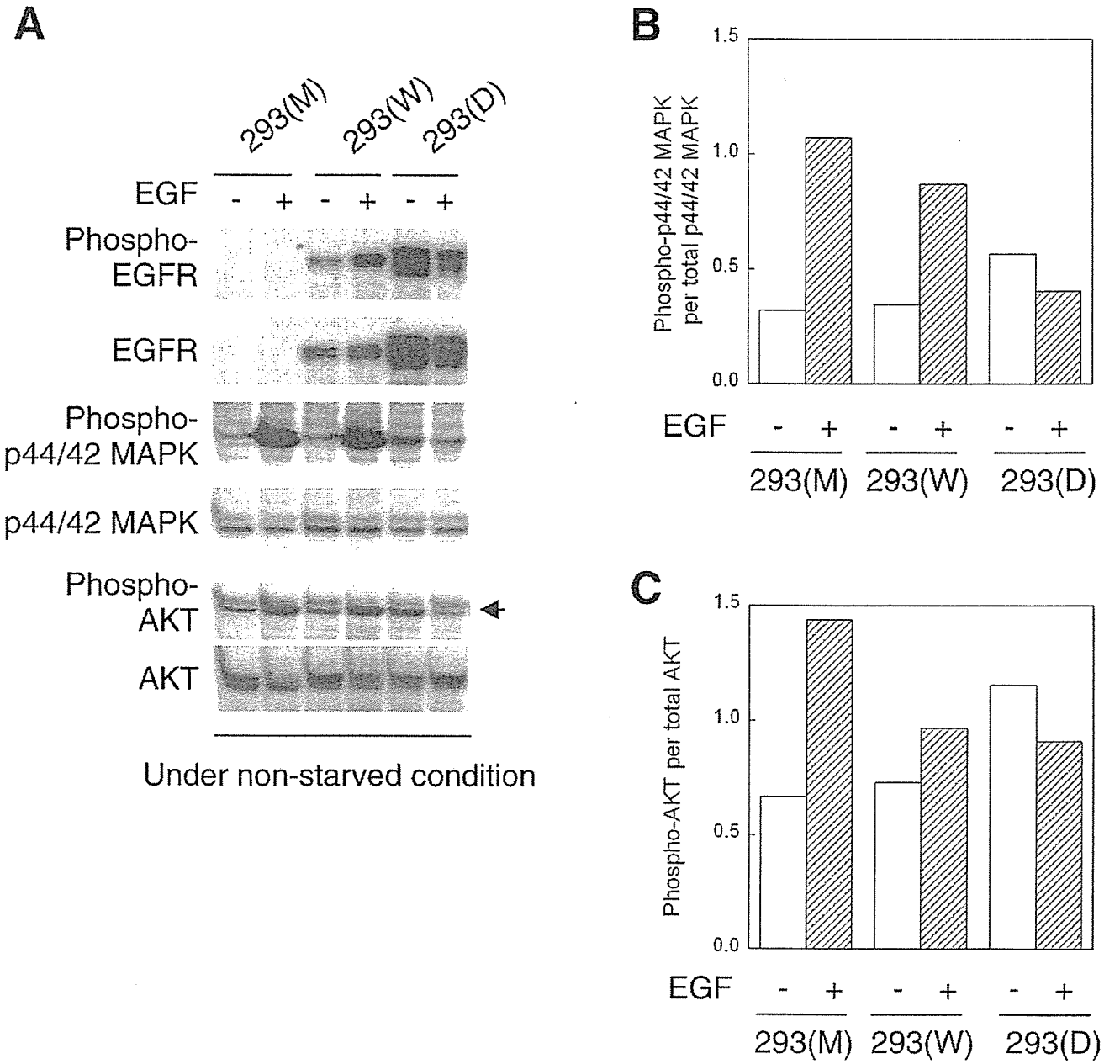

Figure 3. Phosphorylation of EGFR, p44/42 mitogen-activated protein kinase (MAPK), and AKT in the EGFR-transfected 293 cells. ***A***) The 293 (M), 293(W), and 293(D) cells were treated with EGF (10 ng/ml) for 10 min under nonstarved conditions. After two washes with ice-cold PBS(+), monolayer cells were lysed. Equivalent amounts of protein were separated by 2–15% gradient SDS-PAGE for EGFR or 10–20% for p44/42 MAPK, phospho-p44/42 MAPK, AKT, and phospho-AKT, and then subjected to immunoblot analysis. ***B***) Histogram of the degree of p44/42 MAPK activation expressed as phospho-p44/42 MAPK per total p44/42 MAPK. ***C***) Histogram of the degree of AKT activation expressed as phospho-AKT per total AKT.

Fig. 4

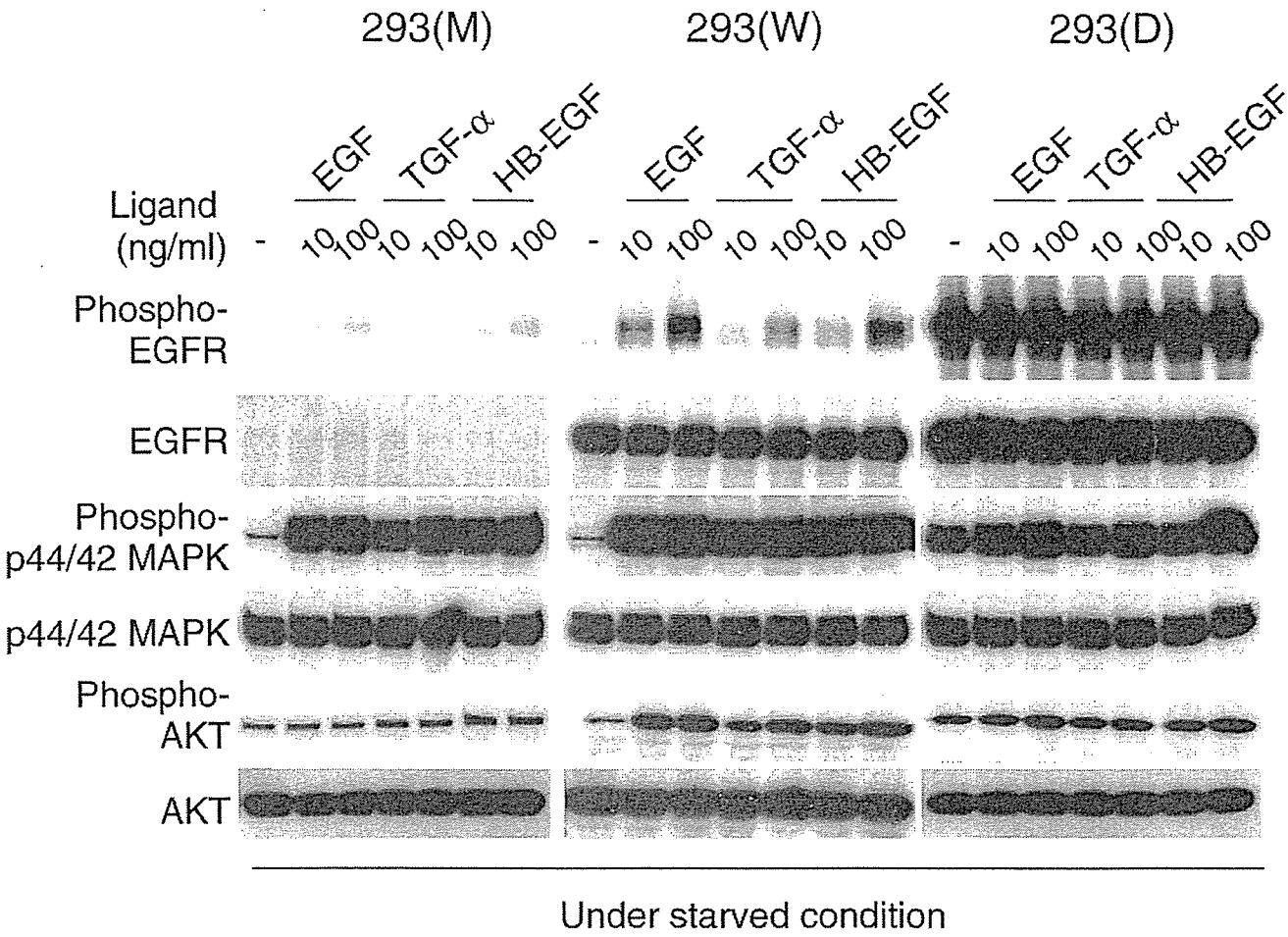

Figure 4. Phosphorylation of EGFR, p44/42 MAPK, and AKT by other ligands. The transfected cells were exposed or not exposed to EGF, TGF-α, and HB-EGF for 10 min under serum-starved conditions. After two washes with ice-cold PBS(+), monolayer cells were lysed. Equivalent amounts of protein were separated by 2–15% gradient SDS-PAGE for EGFR or 10–20% for p44/42 MAPK, phospho-p44/42 MAPK, AKT, and phospho-AKT, and then subjected to immunoblot analysis.